RESEARCH FRONT

CSIRO PUBLISHING

*Journal of Southern Hemisphere Earth Systems Science*, 2020, **70**, 88–105
https://doi.org/10.1071/ES19044

# Atmospheric rivers in the Australia–Asian region under current and future climate in CMIP5 models

*Ying Xu*[A], *Huqiang Zhang*[B,D], *Yanju Liu*[A], *Zhenyu Han*[A] *and Botao Zhou*[C]

[A]National Climate Center, China Meteorological Administration, Beijing, China.
[B]Australian Bureau of Meteorology, GPO Box 1289k, Vic. 3001, Melbourne, Australia.
[C]Collaborative Innovation Center on Forecast and Evaluation of Meteorological Disasters, Nanjing University of Information Science and Technology, Nanjing, China.
[D]Corresponding author. Email: Huqiang.Zhang@bom.gov.au

**Abstract.** Atmospheric rivers (ARs), as long and narrow bands of strong water vapour transport in the lower troposphere, have drawn increasing scientific attention in recent years. Results from a collaborative project between the Australian Bureau of Meteorology and China Meteorological Administration have shown some unique AR characteristics embedded within the Australia–Asian monsoon based on observational analyses. As part of the project, this study focused on assessing the skill of global climate models for simulating ARs in the region under current climate and their projected changes due to global warming. Daily data from 17 Coupled Model Intercomparison Project Phase 5 (CMIP5) models in their historical and Representative Concentration Pathway (RCP) 8.5 simulations were analysed for the periods of 1981–2005 and 2081–2100 respectively. Compared with results derived from European Centre for Medium-Range Weather Forecasts ERA-interim reanalysis data, these model ensemble results showed significant seasonal variations of horizontal water vapour transport as observed, but their magnitudes measured by vertically integrated water vapour transport (IVT) were weaker, particularly for the East Asian summer monsoon. Using an objective AR detection algorithm based on 85th percentile IVT magnitude and its geometry, we showed that multi-model-ensemble (MME) averaged AR occurrence agreed well with the results derived from the reanalysis for their spatial distributions and seasonal variations. Under the RCP8.5 global warming scenario, the model ensembles, overall, showed an enhanced water vapour transport, primarily due to increased atmospheric humidity associated with a warmed atmosphere. Consequently, they simulated increased AR frequency and bigger AR size in most of the region, particularly over north and northeast China and southern Australia. However, the MME results showed a reduced AR frequency and size in July/August in southern and eastern part of China and its adjacent waters. We attributed these results to the response of the Western North Pacific Subtropical High (WNPSH) to global warming. Our analysis showed that westward expansion of WNPSH lead to the shift of ARs more inland in East Asia. In this case, eastern China was directly under the control of WNPSH, which did not favour AR development and penetration into the region. Our analyses of ARs in the A–A monsoon system offers new insight in understanding potential climate changes in the monsoon region under warmed climate.

**Keywords:** atmospheric rivers, Australia-Asian monsoon, CMIP5 models, global warming, moisture transport, Western Pacific Subtropical High.

Received 18 March 2020, accepted 4 August 2020, published online 5 October 2020

## 1 Introduction

As reviewed by Ralph *et al.* (2017), in recent years more and more research has been devoted to studying atmospheric rivers (ARs). They refer to long (expanding well beyond 2000 km in length), shallow (1–2.5 km in depth) and narrow (on average ~500–800 km in width) band of strong water vapour transport in the lower troposphere. ARs usually originate from tropical warm oceans and are often associated with a low-level jet ahead of the cold front of an extratropical cyclonic system (Zhu and Newell 1994; Ralph *et al.* 2004). The increasing interest in ARs is largely due to their close connection with extreme rainfall events in various parts of the globe, particularly in the western coastal regions of North and South America (Dettinger *et al.* 2011; Lavers *et al.* 2011, 2012; Warner *et al.* 2012, 2015; Garreaud 2013; Lavers and Vilarini 2013, 2015; Gershunov *et al.* 2017, 2019; Viale *et al.* 2018; Mo *et al.* 2019), where warm and moist air masses carried by ARs meet with coastal orographic uplift during their landfall (Ralph *et al.* 2004, 2006; Neiman *et al.* 2008*a*, 2008*b*).

Nevertheless, only in recent years do we start to see such research in the Australia–Asian (A–A) monsoon region (e.g. Guan and Waliser 2015; Hirota *et al.* 2016; Paltan *et al.* 2017; Yang *et al.* 2018). Results from a collaborative project between

the China Meteorological Administration (CMA) and the Australian Bureau of Meteorology (BoM), as reported by Ye *et al.* (2020); Chen *et al.* (2020); Xu *et al.* (2020); Liang *et al.* (2020) and Wu *et al.* (2020) in this Research Front, have already revealed some unique features of ARs operating in the region. Results from these studies demonstrated that although an AR is a form of moisture transport, because of its close linkage with specific synoptic patterns in the A–A region and its role in connecting moisture sources in the tropics with weather events in the extratropics, AR diagnosis can help us gain more understanding of detailed characteristics of moisture transport embedded within large-scale monsoonal backgrounds. Key results from these observational AR analyses are briefly summarised below.

Due to different orographic settings and different climatic backgrounds in the region, studies from this collaborative project by Ye *et al.* (2020) and Chen *et al.* (2020) demonstrated that the underlying processes for ARs impacting the weather and climate in the A–A region can be different from the conceptual model developed for North America. The Asian summer monsoon itself is characterised by strong warm and moist air transported from the tropics into extratropical East Asia and nearby waters (Chen *et al.* 1991; Chang *et al.* 2004; Ding 2004; Wang 2006; Zhang 2010). In the case studies of Chen *et al.* (2020) and Xu *et al.* (2020), they pointed out that because China's geographic location is characterised by the Tibetan Plateau to its west, warm oceans to its south and a long coastal line to its east, the prevailing monsoon flow from the Bay of Bengal and South China Sea region propagates northeastward along the hillside of the highlands. Thus, ARs embedded within the monsoon flows travel along the edge of the plateaus rather than directly confronting these high mountains. This is different from the conceptual model applied to the western coast of North America, where landfalling ARs directly encountering high coastal mountains is the primary mechanism for significant rainfall in that region (Ralph *et al.* 2004, 2006; Neiman *et al.* 2008*a*, 2008*b*).

Xu *et al.* (2020); Chen *et al.* (2020) and Wu *et al.* (2020) further showed that ARs, as effective moisture transport mechanisms, played a key role in linking moisture source in the tropics with the synoptics in the middle latitudes. They further showed that the Western North Pacific Subtropical High (WNPSH) played a dominant role in forming ARs in China, whereas in the Australian region, warm and moist air from the eastern part of the tropical Indian Ocean was important for ARs in the western part of the continent. They also explained why ARs in these two regions reached their peaks at the same time but during different seasons through the subtropical high interactions in the western Pacific and Australian region.

Results from Wu *et al.* (2020) and Liang *et al.* (2020) also showed that although ARs are synoptic scale moisture transport mechanisms within the monsoon system, the AR variations are not fully reflected by monsoon circulation intensity, and strong monsoon years do not necessarily mean more ARs. They further showed that due to the large amount of moisture steadily transported by the ARs, AR variations are more closely linked to extreme rainfall variations and their spatial coherence during the East Asian summer monsoon season rather than monsoon rainfall totals.

Furthermore, a critical component of AR research in the A–A region, which deserves more attention, is potential AR changes under a warmed climate (e.g. Payne *et al.* 2020). Indeed, studies have already reported such assessments for other regions. For example, using regional climate model simulations, Jeon *et al.* (2015) reported more ARs and longer durations for the California region. Radić *et al.* (2015) studied the autumn ARs in British Columbia of Canada and suggested that intense AR frequency could increase with global warming. Such results are supported by a recent study by Curry *et al.* (2019), which reported that winter landfall ARs over the British Columbia's Fraser River Basin will increase in both strength and frequency based on Coupled Model Intercomparison Project Phase 5 (CMIP5) model simulations. Lavers *et al.* (2013); Gao *et al.* (2015) and Ramos *et al.* (2016) projected similar results, with increased AR frequencies and risks of intense precipitation in Europe and North America. Nevertheless, there are uncertainties in these projections. For instance, another AR study by Espinoza *et al.* (2018), despite reporting that overall AR frequency increased by ~50% globally, showed considerable intermodel differences in the projected AR changes occurred over different regions, and they called for more research in this area.

Assessing potential AR changes under a warmed climate in the A–A monsoon region is further complicated by several competing processes. Firstly, the A–A monsoon is characterised by significant seasonal changes in prevailing winds and atmospheric moisture. Indeed, Zhang (2010) used a combined atmospheric circulation (850 hPa wind) and moisture (precipitable water) index to capture the A–A monsoon development. These two variables (wind and humidity) are the key variables widely used in AR detections (Zhu and Newell 1998; Lavers *et al.* 2012; Lavers and Villarini 2013; Wick 2014; Guan and Waliser 2015; Mahoney *et al.* 2016; Mo and Lin 2019). Consequently, how atmospheric monsoon circulation and atmospheric moisture condition respond to global warming will determine how the ARs in this region will change in the future climate. By and large, with warmed oceans (more oceanic evaporation, and therefore, enhanced oceanic moisture source to the atmosphere) and warmed atmosphere (increased atmospheric moisture content controlled by the Clausius-Clapeyron rate), we expect increased atmospheric humidity and therefore more favourable atmospheric moisture conditions for the formation of ARs and their intensities under a warmed climate (e.g. Gao *et al.* 2015). On the other hand, how the monsoon will respond to global warming is much less certain (Zhang *et al.* 2012, 2013, 2016; Jiang and Tian 2013; Dong *et al.* 2016), some studies suggested enhanced monsoon circulations whereas others showed a weakened tropical monsoon. As a result, the net offset effects of the changes in atmospheric moisture content and changes in the atmospheric monsoon circulation in the A–A region can potentially lead to different responses of ARs in these models. In fact, Gao *et al.* (2015) already reported some offset effect of wind changes on AR activities against the increase of atmospheric water vapour with warming. Therefore, we need to conduct thorough analyses of how well current climate models simulate the ARs in the A–A monsoon region and how these model project AR potential changes in the future climate. This is the key task of this study. In addition, such a study can help us better understand the trend and variations of 'observational' ARs in eastern China, as reported by Wu *et al.* (2020).

**Table 1. List of the 17 CMIP5 models used in the analysis. Detailed information on the CMIP5 modelling experiments can be found at https://pcmdi.llnl.gov/mips/cmip5/**

| Model | Institution (or group) | Resolution (lon × lat) |
|---|---|---|
| ACCESS1.0 | Commonwealth Scientific and Industrial Research Organisation/Bureau of Meteorology, Australia | 192 × 145 |
| ACCESS1.3 | Commonwealth Scientific and Industrial Research Organisation/Bureau of Meteorology, Australia | 192 × 144 |
| BCC-CSM1–1-m | Beijing Climate Center, China Meteorological Administration | 320 × 160 |
| BNU-ESM | Beijing Normal University, China | 128 × 64 |
| CanESM2 | Canadian Centre for Climate Modelling and Analysis | 128 × 64 |
| CNRM-CM5 | Centre National de Recherches Meteorologiques, Meteo-France | 256 × 128 |
| CSIRO-Mk3-6-0 | Australian Commonwealth Scientific and Industrial Research Organisation | 192 × 96 |
| GFDL-ESM2G | Geophysical Fluid Dynamics Laboratory, USA | 144 × 90 |
| INMCM4 | Institute for Numerical Mathematics, Russia | 180 × 120 |
| IPSL-CM5A-LR | Institut Pierre-Simon Laplace, France | 96 × 96 |
| IPSL-CM5A-MR | Institut Pierre-Simon Laplace, France | 96 × 96 |
| MIROC5 | Model for Interdisciplinary Research on Climate, Japan | 256 × 128 |
| MIROC-ESM | Model for Interdisciplinary Research on Climate, Japan | 128 × 64 |
| MPI-ESM-LR | Max Planck Institute for Meteorology, Germany | 192 × 96 |
| MPI-ESM-MR | Max Planck Institute for Meteorology, Germany | 192 × 96 |
| MRI-CGCM3 | Meteorological Research Institute, Japan | 320 × 160 |
| NorESM1-M | Norwegian Climate Centre | 144 × 96 |

In this paper, we report on our analysis of a suite of CMIP5 model simulations in the A–A region. We firstly assess their skills in simulating atmospheric moisture transport and ARs in the current climate, and then analyse their simulated changes under a future warming scenario. Section 2 introduces the models used and the method we followed to do the AR detections. Section 3 assesses the model skill in simulating ARs in the current climate in the A–A region. Section 4 shows these model-simulated AR changes in a future greenhouse warmed climate and Section 5 presents the main conclusions and discussions. Note that we cannot report on all the aspects of assessing current climate models in simulating ARs in the region within this single manuscript, and separate future studies will be prepared to focus on process analyses and the linkage between potential changes in ARs and their hydrometeorological consequences.

## 2 Models and AR detection methods

As shown in Table 1, in this study we analysed 17 global climate model simulations provided in the CMIP5 experiments (Taylor *et al.* 2012) used for the Intergovernmental Panel on Climate Change Fifth Assessment Report (IPCC 2013). We downloaded the daily atmospheric wind and humidity fields at all the vertical levels from these modelling groups. We used their historical simulations for the 25-year period of 1981–2005 to assess the model skill in simulating AR activities in the A–A region under the current climate. For the AR future projections, we could only analyse these model simulations under the Representative Concentration Pathway (RCP) 8.5 for the 20-year period of 2081–2100 due to the large amount of data to be downloaded and processed. RCP8.5 represents a higher emission scenario for future climate projections (Taylor *et al.* 2012). Detailed model information can be obtained from http://cmip-pcmdi.llnl.gov/cmip5. For the model skill assessment to be consistent with the CMIP5 models, we used ARs derived from the daily averaged six-hourly European Centre for Medium-Range Weather Forecasts ERA-interim reanalysis datasets (Dee *et al.* 2011) for 1981–2005 as our 'observational' reference data.

As pointed out by Ye *et al.* (2020), there are different definitions and thresholds being applied to automatic AR detections (Shields *et al.* 2018). In this study, we selected the method developed by Guan and Waliser (2015). They used the 85th percentile of vertically integrated water vapour transport (IVT) with the geometry requirements of a length >2000 km and length/width ratio >2 as the main thresholds in objectively defining ARs. This method was attractive to us, as our study domain is dominated by the A–A monsoon, which has significant seasonal variations in its prevailing wind and atmospheric moisture conditions (Zhang 2010) and rapid dry-to-wet transitions. Thus, a varying threshold based on percentiles rather than a prescribed quantity is helpful for capturing key features of moisture transport and AR activities within the monsoonal environment. It is our intention in the future to refine and revise this method after we compare our reanalysis-based results with another set of AR databases in the region developed by Wu *et al.* (2020) using manual detections.

The automatic AR detection method of Guan and Waliser (2015) is comprised of the following key components: IVT intensity, IVT directions and IVT band geometry. In our analysis, we did not pay particular attention to the landfall positions, as several studies from this project (Chen *et al.* 2020; Xu *et al.* 2020; Wu *et al.* 2020) have already shown that the influence of ARs on the A–A monsoonal climate was mainly realised by their interactions with middle latitude systems rather than encountering mountains during landfall. The detailed AR detection procedures are given in Guan and Waliser (2015), and below are just some brief descriptions and modifications we applied in this analysis.

(i) We used daily wind components, specific humidity and surface pressure to calculate IVT from surface to the top

of the atmosphere in the ERA-interim and CMIP5 model vertical levels:

$$\mathrm{IVT} = \sqrt{\left(\frac{1}{g}\int_{\mathrm{ps}}^{\mathrm{ptop}} qudp\right)^2 + \left(\frac{1}{g}\int_{\mathrm{ps}}^{\mathrm{ptop}} qvdp\right)^2}$$

where ps is surface pressure, ptop is model's top-level pressure, $q$ is atmospheric specific humidity, and $u$ and $v$ are the zonal and meridional wind components. IVT can also be viewed as the magnitude of the vertically integrated zonal and meridional moisture transport components ($u\times q$; $v\times q$) respectively. Note that although these CMIP5 models provided daily data on standard pressure levels in the lower troposphere, including 1000, 900 and 850 hPa, etc, these results were in fact artificially interpolated from the model surface pressure level (ps) down (or up) to these levels if the surface pressure was lower (or higher) than these standard pressure levels. Considering that most of the atmospheric humidity is concentrated at the low levels of the atmosphere, in the IVT calculations, we needed to integrate from actual surface pressure level rather than the artificial 1000 hPa used in some other studies (e.g. Lavers *et al.* 2015; Warner *et al.* 2015; Gao *et al.* 2015 and Espinoza *et al.* 2018). Therefore, in our analysis, we firstly calculated daily surface pressure from the model mean sea level pressure (MSLP), surface temperature and model altitude data using the following formula from So *et al.* (1994):

$$\mathrm{ps} = \mathrm{psl} \times \left(\frac{\mathrm{tas} + 0.0065 \times \mathrm{zs}}{\mathrm{tas}}\right)^{(-5.257)}$$

where ps is surface pressure, psl is MSLP reported by these models (hPa), zs is the altitude of the model grid (m) at their native resolution and tas is surface air temperature reported by these models (K). This is one of the main differences between our CMIP5 model IVT and AR calculations compared to previous studies (Lavers *et al.* 2012; Gao *et al.* 2015; Espinoza *et al.* 2018) that reported AR analyses and their changes based on IVT calculated from standard pressure levels (1000, 850, 700 and 500 hPa). Another difference is that, in our calculations, the IVT vertical integration started from the surface up to the top-level reported by each of the models, rather than 500 hPa, as used in these previous studies. In a future study, this will allow us to directly compare our results with the ones using precipitable water as the variable in AR detections. The review paper by Ye *et al.* (2020) already discussed the advantage of using IVT over precipitable water in detecting ARs. Nevertheless, in the context of investigating potential changes in ARs under global warming, we plan to conduct another study by comparing results from this study with the ones using precipitable water so we can explore to what extent the changes in ARs are due to the changes in the atmospheric moisture content and in the monsoon circulation. In this study, we only focus on presenting results using IVT calculations.

(ii) We calculated the daily IVT 85th percentile from the 25-year period of the model historical simulations and used it, together with a minimum value of 250 kg m$^{-1}$ s$^{-1}$, as the threshold to identify model grids that satisfying AR IVT requirements.

(iii) We checked the spatial coherence of the model grids, which met the AR IVT requirement to form a band with consistent direction of moisture transport (within 45° variations) as detailed in Guan and Waliser (2015).

(iv) We calculated the geometry of the IVT band, including its axis, length, width and the length/width ratio. To be detected as an AR, the band needed a minimum length of 2000 km and its length/width ratio needed to be great than 2. Note that the use of the minimum value of IVT, together with specific geometric requirements and spatial coherence, helped to reduce the likelihood of a certain model being unable to capture the monsoon circulation, and consequently, miss the northward propagation of the monsoon rain belt but appearing to produce 'realistic' ARs due to the use of percentiles of IVT in the detection. Animation of ARs detected in 1981–2005 using the reanalysis data and a few model results along with rainfall patterns in these datasets also suggested a good representation of the development of synoptic systems accompanied by ARs.

As part of the automatic detection, the frequency, duration and size of ARs were calculated for each month in the A–A region at the model native grids. In this manuscript, we mainly present the results as multi-model-ensemble (MME) averages from these 17 models. In the calculation of MME, we re-gridded the model AR results to a common resolution of 1.125° in latitude by 2.25° in longitude. Because the A–A monsoon owns significant intraseasonal and seasonal variations, we present the results for January, April, July and October to clearly illustrate the AR seasonality in the region. We also present some area-averaged results over several selected regions to explore more detailed regional results.

## 3 Horizontal moisture transport and ARs in the current climate

Fig. 1 compares the model-simulated IVT distributions against the results derived from the ERA-interim reanalysis for the same period. The model results in Fig. 1 are simply the MME mean of the 17 CMIP5 models. It is clear from Fig. 1 that moisture transport in the tropics was largely dominated by zonal wind reversal associated with tropical monsoons, with eastward transport in July for the boreal summer southern Asian monsoon and in January for the austral summer Australian monsoon in its north. Nevertheless, in the AR analysis we focused more on the meridional moisture transport from the tropics into the extratropics. In January, the East Asian land area is dominated by its winter monsoon with strong northeasterly and northwesterly flows over the Eurasian continent (Wang 2006). Nevertheless, IVT calculations revealed that the main moisture source for supporting winter precipitation still came from the south, with large northward moisture transport. This is consistent with other

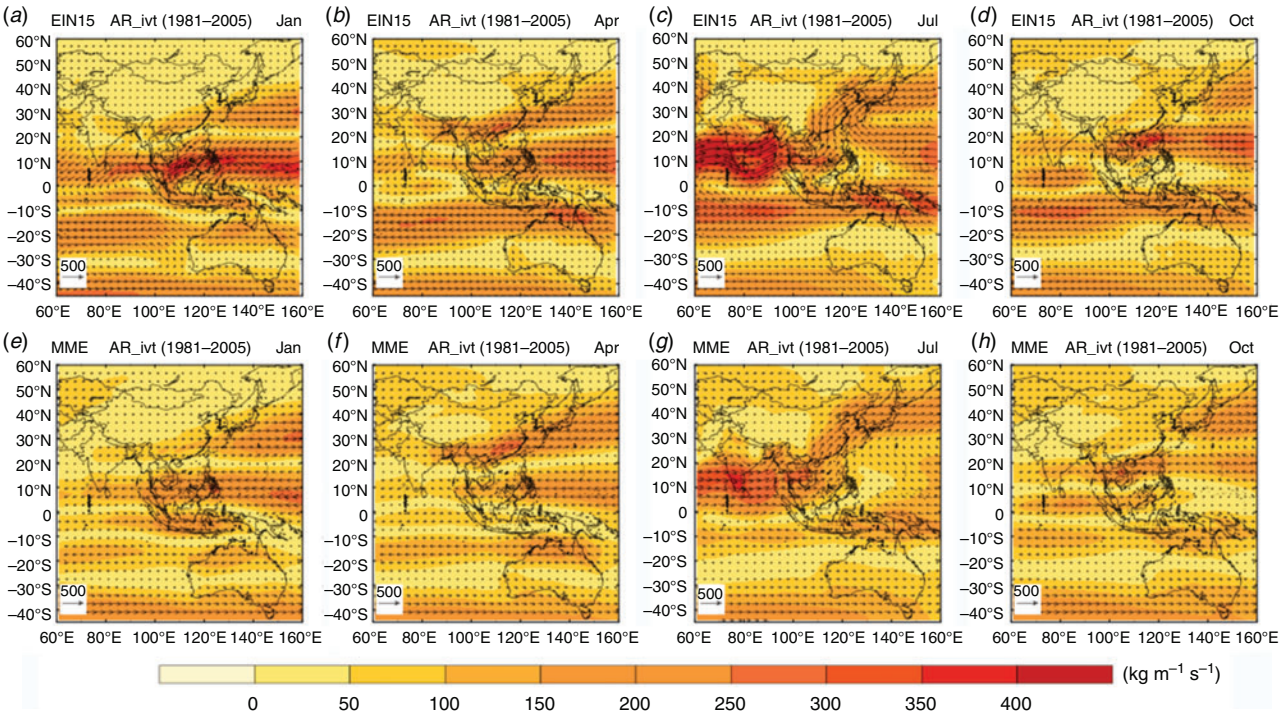


**Fig. 1.** Vertically integrated water vapour transport (IVT) derived from ERA-interim reanalysis data for the period of 1981–2005 for (*a*) January, (*b*) April, (*c*) July and (*d*) October. Shaded colours are the magnitudes of IVT (kg $m^{-1}$ $s^{-1}$), and the vectors are their horizontal zonal and meridional components. (*e–h*) Same as (*a–d*) but for the multi-model-ensemble (MME) averages of the results derived from the 17 CMIP5 models listed in Table 1 for the same period in their historical simulations. See text for details.

studies highlighting the importance of moisture sources from the tropics in determining winter wet and cold climate in the region (Zhang *et al.* 2011). Furthermore, the characteristics of the meridional moisture transport varied with the Asian monsoon development, with enhanced southwesterly moisture transport in April over southern and eastern parts of the continent. When the summer monsoon was further established, strong southwesterly moisture flow associated with South Asian monsoon and southeasterly moisture flow associated with the WNPSH dominated the East Asian land and nearby waters. During these months, tropical moisture could be transported into the far northeast part of China and then turned eastward into Japan and the Korean peninsula, leading to heavy rainfalls over these regions. Such moisture transport pathways have been documented in the AR case studies of Chen *et al.* (2020); Xu *et al.* (2020) and Wu *et al.* (2020).

The IVT spatial patterns and their seasonal variations in the East Asia and nearby regions were successfully represented in the MME of the 17 models, but with weaker intensities. This is consistent with many other studies that suggested current CMIP models tend to simulate a weaker monsoon circulation than observed (IPCC, 2013; Jiang *et al.* 2016). It needs to be pointed out that because the AR detection in this study used 85th percentile IVT values rather than a fixed IVT threshold, the impacts of such systematic model biases shown in Fig. 1 and in other studies (e.g. Gao *et al.* 2015; Espinoza *et al.* 2018) were less severe in our AR detection, as we show later. This was indeed the reason why we chose this method from Guan and Waliser (2015) in the analysis.

In tropical Australia, horizontal atmospheric moisture transport was largely dominated by easterly to westerly zonal wind reversal associated with the Australian monsoon. Compared with the results for tropical Asian monsoon, its intensity was much weaker (Zhang and Moise 2016). Over the Australian continent, meridional moisture transport mainly occurred in the middle latitudes south of 20°S. Comparing IVT results in January, April, July and October, the IVT magnitudes tended to be larger during the months of July and October. This was largely associated with the equatorward retreat of the Australian subtropical high during the austral winter (boreal summer) months, as discussed in Xu *et al.* (2020). In that study, they showed a close connection between the north–south shifts of the WNPSH and the subtropical high in the southern hemisphere. This close connection explains why ARs reach their peaks during the same period in both regions. Furthermore, the model-simulated IVT biases were less severe than in the East Asian land mass and nearby waters.

The frequency of AR occurrence in the A–A region is shown in Fig. 2. The frequency at each model grid was calculated as the averaged total number of ARs that occurred at the grid during the 25-year period of 1981–2005 at each month. Note that a single AR event could remain at the same location for several days during its development and movement. There are several interesting results shown in this figure:

(i) Although the largest IVT mainly occurred in the tropics, as shown in Fig. 1 (roughly between the 10°N and 10°S band), the regions with high AR occurrence were in both middle

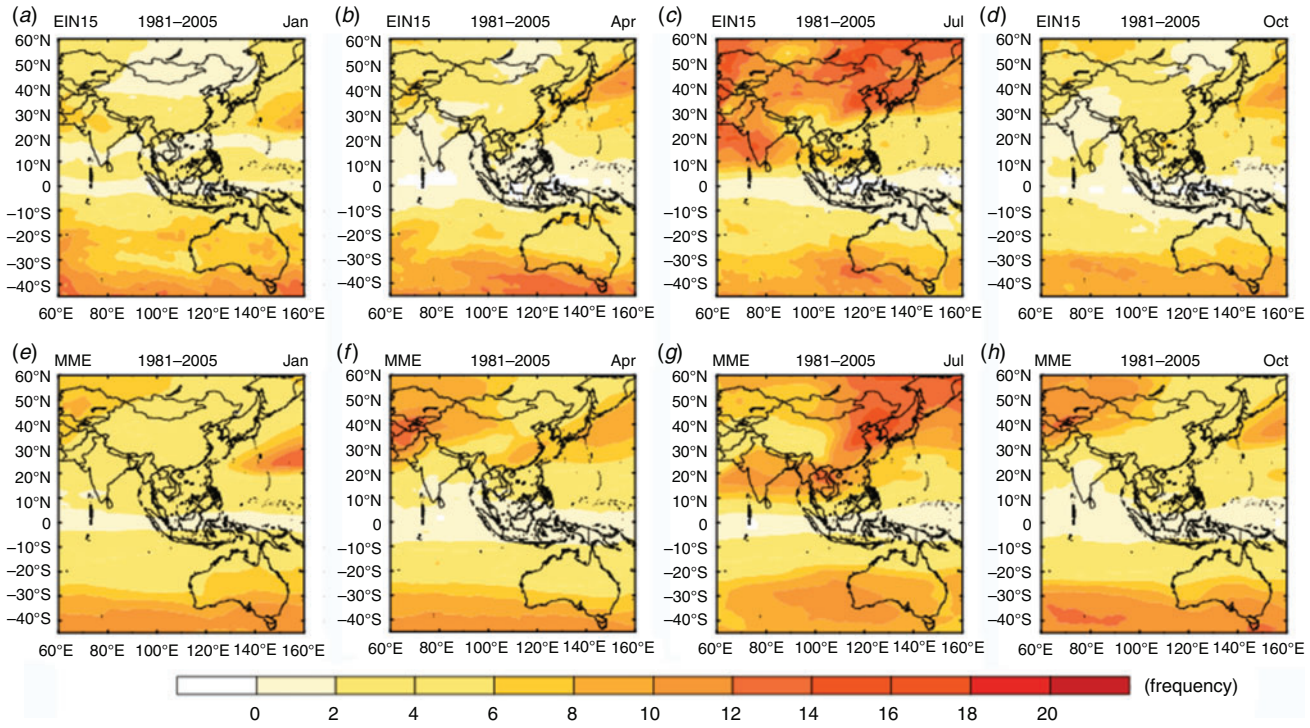


**Fig. 2.** AR frequency derived from ERA-interim reanalysis data for the period of 1981–2005 for (*a*) January, (*b*) April, (*c*) July and (*d*) October. The frequency shown in the figure is the total number of days for that month with ARs being detected at each grid. (*e–h*) Same as (*a–d*) row but for the MME averages of results derived from the 17 CMIP5 models listed in Table 1 for the same period in their historical run. See text for details.

latitudes. The highest AR occurrence in the Asian region was in northeastern China and far northeastern Asia (including Japan, Korea and nearby seas) and part of northwest Pacific. The largest occurrence in the Australian and nearby regions was over the southern part of the Australian continent and nearby waters. This reflects the fact that ARs are mainly responsible for the moisture transport from the tropics into the subtropics and middle latitudes.

(ii) As shown in Guan and Waliser (2015), the East Asian continent indeed had a low frequency of AR occurrence during most of the year, but it had a higher occurrence in July in Fig. 2 during the peak of the boreal summer monsoon. During this month, significant ARs existed over the Indian subcontinent, which has been reported in some case studies (Yang *et al.* 2018), and in North and East Asia. North and northeast China, and Japan and the Korean peninsula had the highest numbers of ARs. As discussed before, this high number of AR occurrences was related to the northward migration of the WNPSH in the boreal summer. CMIP5 MME successfully captured these features. Although ARs in the monsoon region are linked to monsoon circulations, some of the AR characteristics cannot be represented by monsoonal circulation alone. In Fig. 1 we see intense moisture transport (IVT) in southeast Asia, southern China and tropical western Pacific during the peak of the Asian monsoon in July, but the frequency of AR occurrence in these regions was low. This can be understood as such that the Asian summer monsoon establishment in the region provided a large-scale background that shifted the warm and moist tropical environment further northward. The ARs operating within the monsoon system then created further northward moisture transport into middle–high latitudes. This northward moisture transport linked the tropic systems with extratropical weather, which often generates extensive rainfall. The spatial patterns of the MME AR occurrence, their seasonal variations in Fig. 2 and their spatial variations were highly comparable to the ERA-interim results. In the Australian region, Fig. 2 shows a higher number of ARs over the Australian continent in its austral cool months in July and October. Both the reanalysis and MME data results in July further suggested a higher frequency of ARs in Western Australia. As extensively discussed in Ye *et al.* (2020) and Wu *et al.* (2020), such seasonality and spatial distribution agree with the observed spatial and temperature variations of Northwest Cloud Band influencing Australia.

(iii) Although the MME tended to underestimate the magnitudes of IVT, as in Fig. 1, their AR frequency did not show a systematic bias. In some cases, the AR frequency was even higher in MME than in the reanalysis data, including locations over the northwest Pacific in January and over southwest and southeast Australia in July and October. This was partly due the fact that varying IVT thresholds (based on the 85th percentile values of IVT magnitudes) were used in the AR detection (Guan and Waliser 2015),

as described in Section 2. This can partly ease the deficiency of CMIP5 model biases in their simulated horizontal moisture transport (IVT) used in AR detections.

(iv) Overall, Fig. 2 shows encouraging results about the MME skill of these CMIP5 models in reproducing the 'observed' AR distributions in the A–A region based on the ERA-interim reanalysis data. Their seasonal variations, which will be further discussed in the next section for area-averaged changes, were also well captured. This gave us the confidence to use these MME results to investigate potential AR changes in a future warmed climate.

## 4 Potential changes in IVT and ARs in the A–A region

Assessing potential changes of the monsoon climate in the A–A region has long been a key task in regional and global climate change projections (IPCC 2007, 2013). Nevertheless, it is still a grand challenge to produce reliable projections. This is because the complexity of the monsoon system is governed by a range of dynamic and thermodynamic processes (Wang 2006; Zhang and Moise 2016). This results in large uncertainties in Coupled Model Intercomparison Project Phase 3 (CMIP3) and CMIP5 projections. A review by Kitoh (2017) on the Asian monsoon suggested that CMIP3 and CMIP5 models gave similar future projections: increases in precipitation but weakened circulation for South Asian summer monsoon and enhanced circulation and increased precipitation for the East Asian summer monsoon. The compensating dynamical and thermodynamic effects of increased greenhouse gases and aerosol forcing in the region also contributed to the uncertainty of projected monsoon climate in a future warmed climate (e.g. Li *et al.* 2015). Considering that AR and IVT analyses are essentially the analyses of vertically integrated $u\times q$ and $v\times q$ explains why an AR analysis is helpful to understand the combined effects of changes in the monsoon circulation ($u$, $v$, i.e. dynamics) and changes in the atmospheric moisture content ($q$, influencing thermodynamics) on the monsoon climate.

Prior to the assessment of changes in ARs, we firstly examined how the atmospheric moisture transport changed in the CMIP5 model simulations. Fig. 3 shows the 20-year MME IVT changes in January, April, July and October between the mean of 2081–2100 under RCP8.5 and 1986–2005 historical simulations. The changes in the IVT magnitudes are shown as shaded colours in percentage values (changes relative to the values in the historical simulations). The vectors show the changes in zonal and meridional components of IVT. Firstly, regardless of the months and regions over most of the A–A domain, the MME and IVT variations all showed an increase in IVT magnitude, and this largely contributed to the increase in atmospheric water vapour content due to warmed atmosphere (Lavers *et al.* 2015; Gao *et al.* 2015). Secondly, subtropical regions had relatively weak increases in IVT, particularly over the East Asian monsoon region (southern China and eastern China), tropical western Pacific, southern part of Australia and its nearby oceans. As to be discussed later, the weak changes in IVT over East Asian land can be explained by weak changes and a spatial shift of the meridional monsoon circulation penetrating these regions. In the boreal winter months (January and October), a weakened Asian winter monsoon under global warming (Zhang and Zhang 2010) also means relatively small changes in IVT in the Asian region.

Over the Australian region, there were some different features from what were seen in the Asian region. In January (its summer monsoon period), there were only moderate increases in IVT due to the compensating effect of the enhanced atmospheric water vapour content under a warmed climate and weakened Australian monsoon westerlies, as shown in studies such as Zhang and Moise (2016). This was shown as anomalous eastward IVT changes in tropical Australia in Fig. 3. At the same time, we tended to see an enhanced anticyclonic IVT pattern over most of the Australian continent outside of the tropics. As revealed in the study of Xu *et al.* (2020), this anticlockwise IVT setup favours the formation of ARs in the Australian continent. The enhanced northwest–southeast penetration of tropical moisture into the western part of the continent could lead to increased AR activities in the future, as to be explained next.

Corresponding to the changes in IVT, the potential changes in AR occurrences in the A–A region are shown in Fig. 4. The results are presented as fractional changes in AR frequency against the mean value from their historical simulations. Because of specific requirements of the IVT field used in detecting ARs, the overall enhanced IVT under a warmed climate seen in Fig. 3 does not necessarily mean the same patterns of changes occurred in ARs. In the East Asia land regions and nearby waters, one of the most significant changes was the increased AR frequency in north and northeast China and Japan and the Korean peninsula. This increase was also shown in the analysis of Espinoza *et al.* (2018). The magnitude of this increase was consistent with Gao *et al.* (2015) who also reported an increase in the range of 50% to more than six times in the middle–high latitudes of western North America. Note that some of the very high fractional increases were largely caused by the expansion of the regions where ARs can occur rather than significant increases in AR numbers in RCP8.5. This can be understood as such that for regions with very low AR frequency in their historical simulations, a small increase in AR numbers under RCP8.5 could lead to very high AR fractional changes because of a very small denominator in the fraction calculations. Secondly, the underlying reason for this significant increase was largely attributed to the increase in atmospheric water vapour content associated with warmed atmosphere. This means the same atmospheric circulation condition could have carried more water vapour into these middle latitude regions, which led to more AR occurrences; however, in this study, we did not explicitly decompose the net AR changes into contributions by thermodynamic and dynamics changes, as done by Gao *et al.* (2015). Their analysis of CMIP5 models indeed suggested that such AR increases were predominantly controlled by the super-Clausius-Clapeyron rate of increase of atmospheric water vapour with warming, whereas changes of winds that transport moisture in the ARs, or the dynamical effect, mostly countered the thermodynamical effect of increasing water vapour, thereby limiting the increase of AR events in the future.

Nevertheless, the potential changes in AR frequency in the boreal summer month (July) showed some notably different features compared with other months (Fig. 4). These changes in July were also different from results reported by other studies in

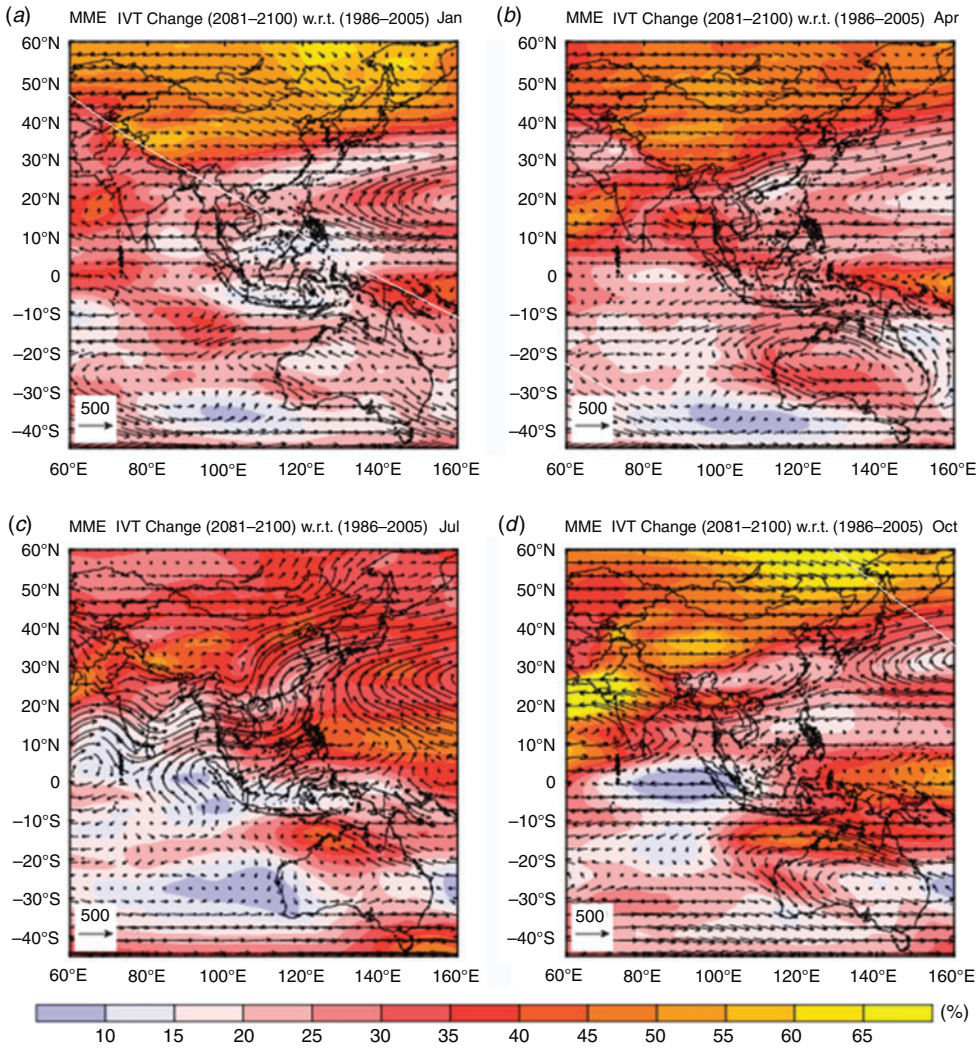


**Fig. 3.** MME averaged changes in the magnitudes of IVT (in percentage against its historical runs and shown by shaded colours) and changes in its zonal and meridional components (kg $m^{-1}$ $s^{-1}$ and in vectors) in (*a*) January, (*b*) April, (*c*) July and (*d*) October between the results derived from 2081–2100 in the models' RCP8.5 runs against the mean for the period of 1986–2005 in their historical runs.

other parts of the globe (e.g. Gao *et al.* 2015; Lavers *et al.* 2015 and Espinoza *et al.* 2018). Based on these 17 model MME, we saw a weak decrease over the eastern part of China, Yellow Sea, Bohai Sea, Korean Bay and part of the northwest tropical Pacific. To the west of these decreases, we saw small increases towards the East Asian inland region. Combing these changes, they tended to suggest a westward inland shift of ARs in the subtropical East Asia monsoon domain. These results are very different from results reported for other extratropical regions (e.g. Warner *et al.* 2015; Lavers *et al.* 2015; Gao *et al.* 2015; Espinoza *et al.* 2018), which showed an overall increase in annual total AR occurrences.

A few questions then arise regarding to such results in East Asia. The first question is whether we saw a trend in the observed ARs over the region that showed similar variations as the model simulations, given the fact that we have already experienced unequivocal warming in the last half century (IPCC 2007, 2013). Although there are significant caveats in directly using observational results to support results from model simulations without comparing detailed processes, such an agreement would prompt further investigation to consolidate these model results. Indeed, from the 30-year AR datasets in China developed by manual detections reported by Wu *et al.* (2020), which were also based on IVT analysis, they reported a significant downward trend of AR frequency over the eastern part of China for the period of 1981–2016. Furthermore, they noted that the downward trend of manually detected ARs in eastern China was in agreement with the changes in the extreme rainfall characteristics over that region, including reduced rainfall extremes and reduced spatial coherence of extreme rainfall events (Ding *et al.* 2020). Therefore, the reduction of AR frequency in these MME, supported by some observational evidences in AR and extreme rainfall analysis, warrants more detailed analyses in our future research to

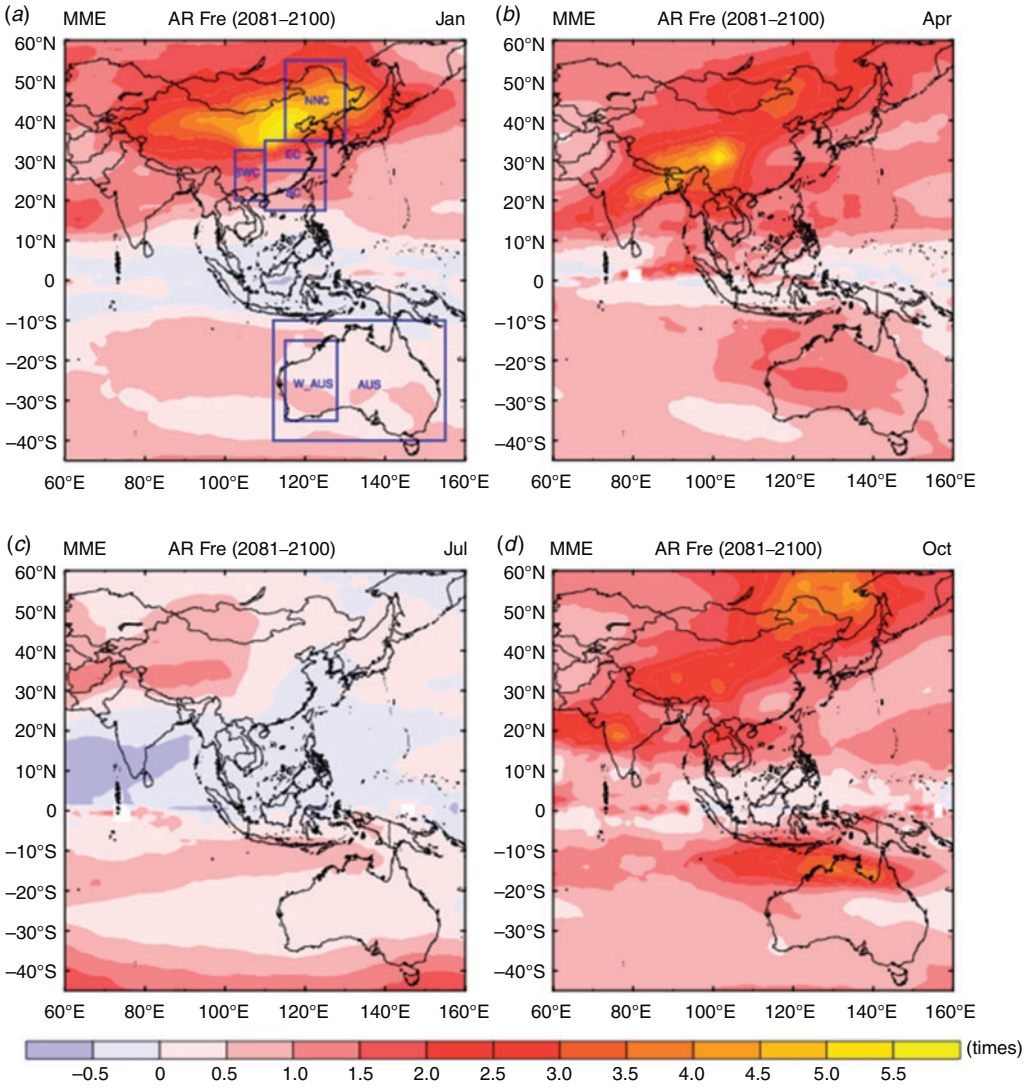


**Fig. 4.** Changes in the AR frequency for the months in (*a*) January, (*b*) April, (*c*) July and (*d*) October for the period of 2081–2100 in the models' RCP8.5 runs against the results for the period of 1986–2005 in their historical runs. The results are presented as fractional changes against the mean value from the historical runs (unitless). The thick blue rectangles in (*a*) represent the area-averaged used in producing the box and whisker plots to be shown in Fig. 6.

further explore the linkage between changes in ARs and changes in rainfall extremes in the region. Such analyses will include examining trends in atmospheric circulation in the model simulations and observations, changes in atmospheric moisture conditions and changes in the Meiyu frontal systems during the East Asian summer monsoon, which transform moisture fed into the region through ARs into rainfall.

Although these changes in July were weak, we still need to investigate possible underlying processes leading to such changes. Considering the fact that ARs in East Asia are significantly affected by the WNPSH, as shown by the studies from Chen *et al.* (2020); Xu *et al.* (2020) and Wu *et al.* (2020) in this project, we examined how the WNPSH could be potentially changed by global warming, as simulated in the CMIP5 models. There have been many detailed studies on this. Firstly, observational studies, such as Zhou *et al.* (2009), showed a westward extension of the WNPSH since the late 1970s, partly due to the contrast of changes in atmospheric diabetic heating between the Indian Ocean and western Pacific. A recent observational study by Choi and Kim (2019) also showed a thickened WNPSH due to global warming that was stronger and shifting more towards the Asian continent. As discussed in Wu *et al.* (2020), such a shift would favour more ARs towards the inland west of the eastern China. However, projection studies based on CMIP model outputs for assessing potential WNPSH changes under future climate are still inconclusive (He and Zhou 2015); some studies have claimed an intensification and westward extension of the WNPSH (Seo *et al.* 2013; Liu *et al.* 2014), whereas others have argued that WNPSH will remain generally unchanged (He *et al.* 2015).

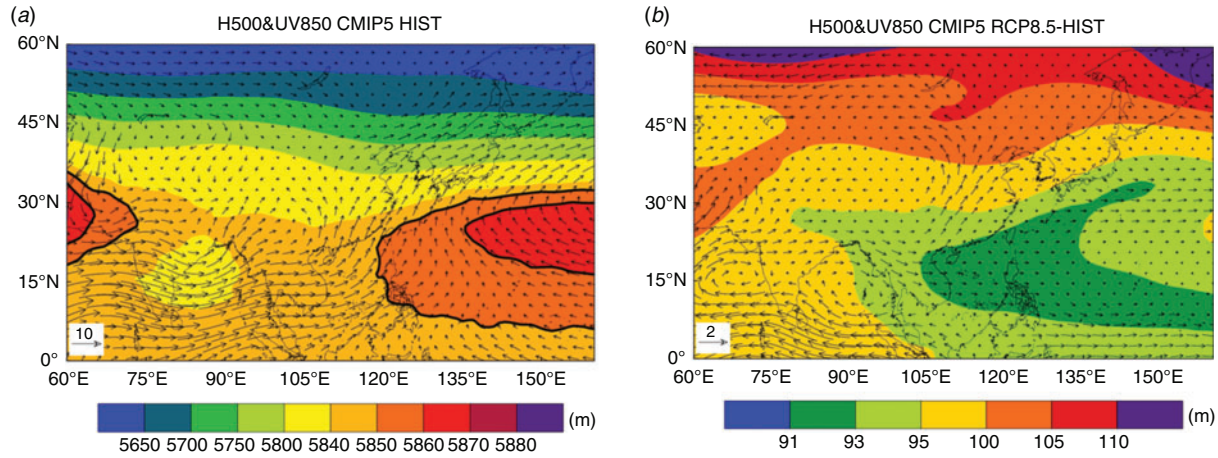


**Fig. 5.** (*a*) MME of 500 hPa geopotential height (shaded colours and contour lines with unit of m) in July simulated by the 17 CMIP5 models historical run for the period of 1986–2005 and their corresponding 850 hPa wind ($ms^{-1}$). The two black, thick, solid lines are the contour lines of 5850 m and 5860 m. (*b*) As for (*a*) but for the MME of changes between RCP8.5 July results for 2081–2100 and results in (*a*).

Although our study did not focus on the WNPSH itself, here we present a simple analysis of the potential changes of WNPSH in the 17 CMIP5 models used in this analysis. As shown in Fig. 5*a*, the MME of these models' historical simulations clearly demonstrates that the meridional monsoon flow from the tropics into the East Asian subtropical monsoon domain was largely controlled by the position and intensity of the WNPSH, with its western flank characterised by strong south/southwesterly winds. Within such a large-scale monsoonal circulation background, ARs were formed and provided an important mechanism for effectively transporting warm and moist air into the East Asian region, as illustrated in Chen *et al.* (2020) and Wu *et al.* (2020). Fig. 5*b* shows changes in 500 hPa height and 850 hPa winds under a RCP8.5 warmed climate. We chose 850 hPa wind because a large part of the atmospheric water vapour transport is concentrated in the lower troposphere, while 500 hPa is the classic height for measuring WNPSH (Wang 2006). Firstly, Fig. 5*b* shows an enhanced WNPSH by large increases in the 500 hPa geopotential height, with more than a 90-m increase of the atmospheric thickness over the whole domain. Secondly, the shape of the increase in the tropical western Pacific also shared similar features with the shape of WNPSH shown in Fig. 5*a*. Combining these features together, results tended to suggest a westward extension of the WNPSH, as reported by Seo *et al.* (2013) and Liu *et al.* (2014). Associated with the shift, one can clearly see in Fig. 5*b* an inland shift of the 850 hPa monsoonal south/southwesterly winds from eastern China in the historical simulations to the west towards central China under RCP8.5 conditions. It also penetrated further northward into north-northeast China and far northeastern Asia. Meanwhile, as pointed out by He *et al.* (2015), changes in 500 hPa geopotential height gradient are important for understanding wind changes within the WNPSH. For regions located directly underneath the WNPSH in the tropical western Pacific and eastern China, their meridional wind was even slightly weakened in RCP8.5 conditions. The offshore wind anomalies in south and eastern China in Fig. 5*b* were linked to the reduced zonal pressure gradient in the region (i.e. the geopotential height increases within the WNPSH were less than in its west). Then, we used these changes presented in Fig. 5*b* to explain the changes in AR frequency shown in Fig. 4: (i) the weak increase in AR frequency in central and central-west China in July was consistent with the inland shift of the monsoonal south-southwesterly flows, as shown in Fig. 5*b*; (ii) in eastern China, which was located underneath the influence of westward-shifted WNPSH, the dryer and warmer air mass caused by the deep anticyclonic system and the anomalous offshore westward wind did not favour AR formation and penetration, resulting in a weak reduction in AR frequency in south and eastern China in July, as shown in Fig. 4. Indeed, a recent study by Kamae *et al.* (2019) also pointed out that some of the differences in model-project changes in East Asian ARs were partly related to the spreads of the WNPSH responses in these models. This is consistent with the ensemble results here. In a future detailed analysis, we need to further explore the changes in ARs in East Asia to the changes both the North Pacific High and the WNPSH. We also need to further separate out changes in the monsoon circulation, changes in the atmospheric moisture content and changes in the vertical structure of the monsoon circulation to strengthen the analysis presented here.

In the Australian region, the 17 CMIP5 model ensembles simulated only weak increases in January and July. Only in April and October, during the transition season, did we see some notable changes. In April, the models showed an increase in AR frequency, especially in the western and central area of the continent. This increase was associated with an enhanced anticyclonic IVT pattern dominating the continent (Fig. 3). As discussed in Xu *et al.* (2020) and Wu *et al.* (2020), this anticyclonic pattern is a critical component for the formation of ARs over the Australian continent. The northwesterly flow associated with the IVT pattern, interacting with an enhanced middle latitude trough southwest of the continent, provided a favourable background for more AR occurrences. Similar patterns of changes in IVT over Australia in October also corresponded to the increases of AR frequency over the north and western part of the continent. Furthermore, the large changes in October–December also

correspond to a period of most frequent extratropical teleconnection for monsoon bursts (Narsey *et al.* 2017). The changes in the background state could be more conducive to extratropical Rossby wave refraction and induced such circulation patterns favourable to the ARs. Such a hypothesis warrants further investigation. In addition, with the increased ARs in both April and October, such results tended to suggest an extended AR season in the region, considering that both observations (Wu *et al.* 2020) and these CMIP5 model simulations (Fig. 5) display a relatively peak AR season of May–September over the continent.

To further display some detailed regional features, as well as to estimate uncertainty in these model simulations, Fig. 6 shows the box and whisker plots for several regions averaged over China and Australia. The regions used in the calculations are shown in Fig. 4*a*. In China, there were four regions selected: (i) north-northeast China (China_NNC: 35°N–55°N, 115°E–130°E) where the models showed significant increases in AR frequency; (ii) eastern China (China_EC: 27.5°N–35°N, 110°E–125°E), largely over the middle and lower reaches of the Yangtze River region where the climate is characterised by boreal summer Meiyu phenomenon and extreme rainfall intensity and spatial coherence has dropped in recent decades (Ding *et al.* 2020), and where observational AR analysis over China has also shown a significant downward trend (Wu *et al.* 2020); (iii) southern China (China_SC: 17.5°N–27.5°N, 110°E–120°E); and (iv) southwest China (China_SWC: 20°N–32.5°N, 102.5 °E–110 °E). We compared the AR frequency derived from ERA-interim data, the corresponding results derived from the 17 CMIP5 models' historical simulations and their simulations using the RCP8.5 scenario. Such results also allowed us to assess the model skill in capturing the AR seasonality over these regions and their changes in a warmed climate. Note that to complement the information in Fig. 4, which shows the fractional changes in AR frequencies in the A–A region, we presented the quantities of the ARs in the historical and RCP8.5 simulations in Fig. 6.

In southern China (17.5°N–27.5°N, 110°E–120°E), the AR frequency peaked in June, whereas the peak arrived a month later (July) in eastern China. During the late monsoon season (July and August) we saw a dramatic increase in AR frequency in north and northeast China. These intraseasonal variations of the AR activity were in good agreement with the pronounced northward jump of its monsoon rainfall belt during the course of the East Asian monsoon development. The CMIP5 MME, overall, agreed well with the AR seasonality derived from the reanalysis results. The averaged total number of ARs derived from the reanalysis data were located within the whisker boxes of the 17 model MME, suggesting a reasonable performance of these model ensembles in capturing ARs in the Asian monsoon climate and their seasonal variations.

Under global warming, AR frequency showed notable increases over East Asia and nearby regions in most of the months. Of the four regions shown in Fig. 6, north-northeast China showed the most significant increases, and such results were consistent with what have been reported in other middle latitude regions (Gao *et al.* 2015; Espinoza *et al.* 2018). In general, more AR occurrence was projected for most of the months in most regions, but in the months of July and August (peak months of the East Asian monsoon), these models showed a reduced AR occurrence in July in southern China and eastern China, likely caused by weakened and shifted monsoon meridional circulations associated with changes in the strength and positions of WNPSH, as illustrated in Fig. 5.

In the Australian region, Fig. 6 shows a weak seasonal cycle of the AR frequency with a tendency of more ARs occurring in the austral cool months of May–September. This seasonality was more evident in the results averaged over the western part of the continent. As extensively discussed in Wu *et al.* (2020), observational AR datasets also confirm such a seasonality. The study by Xu *et al.* (2020) further proposed that a close connection between WNPSH in the northern hemisphere and its southern hemisphere counterpart (the Australian subtropical high) is the chief reason why the ARs tend to peak at the same time but during different seasons in both East Asia and Australia. Under global warming, the 17 CMIP5 models showed an overall increase in AR frequency over the Australian continent. The increase was relatively larger in its warmer months, leading to weakened seasonal variations under a warmed climate.

Although this analysis focused on the AR frequency and its changes simulated by these CMIP5 models, here we also briefly present some results on the possible changes of AR size in a warmed climate. In Fig. 7, the AR size was calculated as the multiyear averages of the total area of model grid boxes (both land and sea) located within each AR event during the period, as used in Guan and Waliser (2015). In the East Asian region, we saw the same tendency of changes in AR frequency and its size: more and bigger ARs are expected under a warmed climate in East Asia in most of the months except for the peak monsoon months of July and August. During these two months, we saw slightly reduced AR sizes in southern and eastern part of China. In the Australian region, most of the models showed a weak increase in the AR size, whereas ARs become bigger in October–December.

While the whisker-box plots in Figs 6 and 7 indicate some uncertainty in the analysis of AR changes simulated by these 17 models, in Fig. 8 we further show the intermodel root-mean-square deviations against the MME of changes simulated by these models. We followed a method used by Li and Zhou (2010) in assessing uncertainty in climate change projections, calculated as:

$$S_x = \sqrt{\frac{1}{n}\sum_{i=1}^{n}(M_i - MME)^2}$$

where Mi is changes simulated by model i, MME is the multi-model-ensemble averaged changes and n is the total model number (n=17 in this analysis). Thus, the larger the results, the larger the intermodel differences, and therefore, the larger uncertainty in these model projections. Overall, we saw the large signal of the AR changes in north-northeast China (except for July), eastern China and southern China (except for July) and the changes in most of the Australian region as less uncertain than the results projected over the Tibetan Plateau and the central Eurasian continent. It is widely acknowledged that modelling the climate system over the Tibetan Plateau and the central Asia region (Zhao and Zhang 2016) requires high resolution (both horizontal and vertical) and sophisticated processes to adequately represent the complex terrain and land–air interactions over these regions. For the AR analysis, the error of calculating surface pressure based on

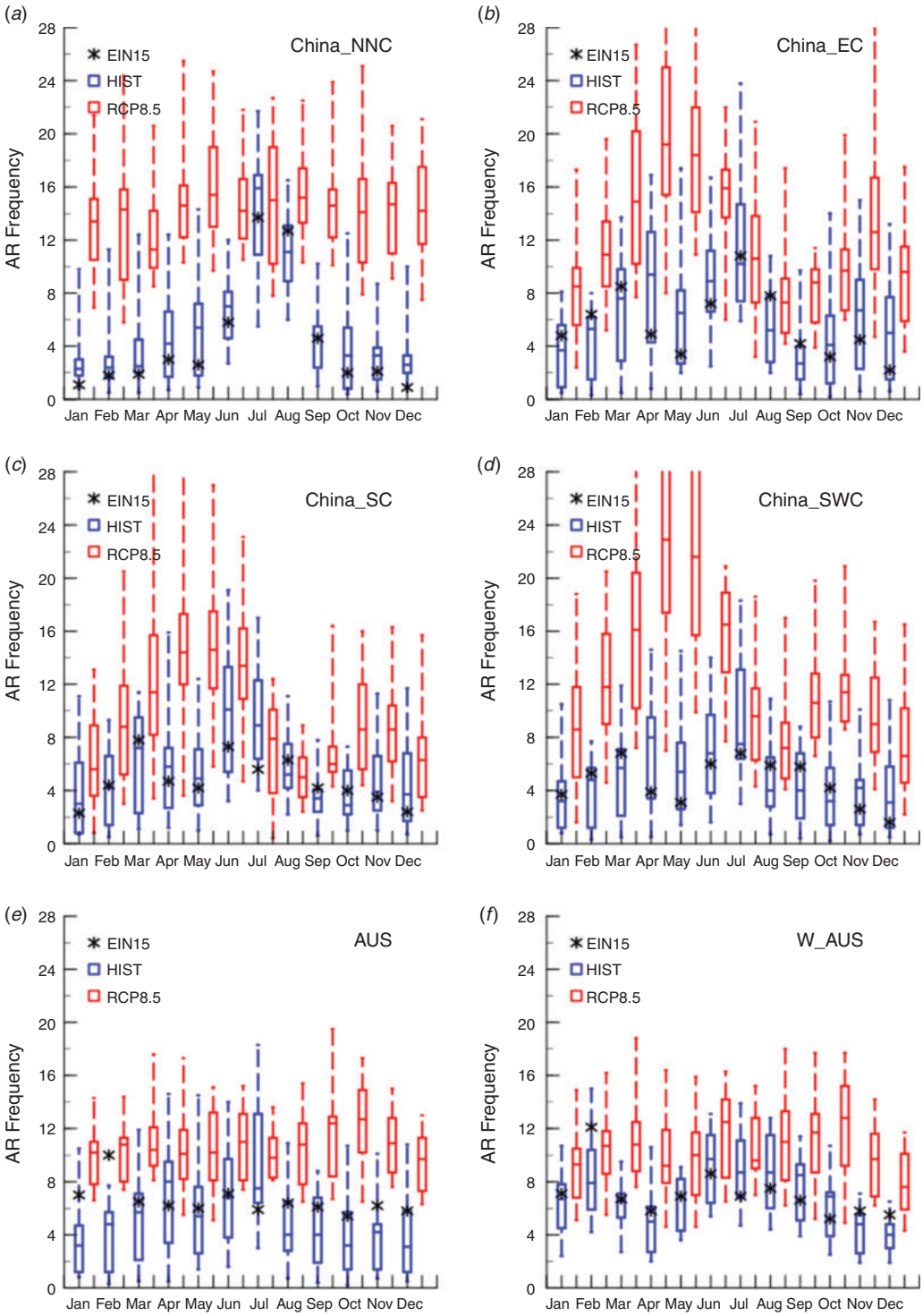


**Fig. 6.** Box and whisker plots for area-averaged AR frequency from ERA-interim reanalysis (* symbol) 17 CMIP7 model's historical run (blue colour) and RCP8.5 run (red colour). The six regions are: (*a*) north-northeast China (China_NNC: 35°N–55°N,115°E–130°E); (*b*) eastern China (China_EC: 27.5°N–35°N, 110°E–125°E); (*c*) southern China (China_SC: 17.5°N~27.5°N,110°E~120°E); (*d*) southwest China (China_SWC: 20°N–32.5°N, 102.5 °E–110 °E); (*e*) whole Australian region (AUS: 40°S–10°S, 110°E–155°E) and (*f*) Western Australia (W_AUS:35°S–15°S, 115°E–128°E). The domains are shown in Fig. 4*a* as blue rectangles.

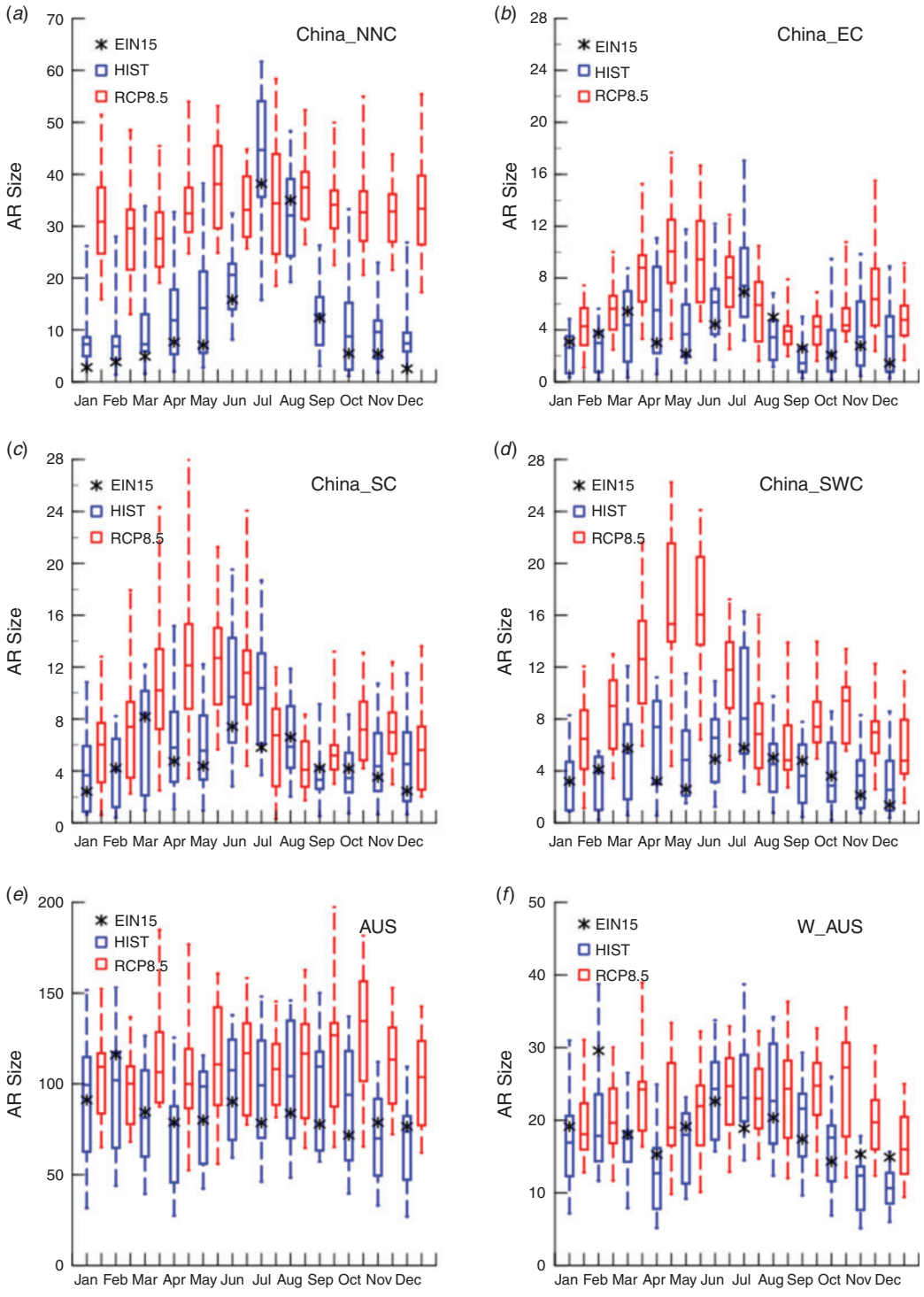


**Fig. 7.** As for Fig. 6 but for the AR size, which is calculated as the total area of the model grid boxes within each AR event. Unit: $km^2$.

the model reported MSLP and surface air temperature could have also added uncertainty to IVT calculations in these highland regions. As a result, we saw a large uncertainty over these regions for the projected changes in ARs.

## 5 Summary and discussions

As part of the collaborative project between the BoM and CMA on AR studies in the A–A region (Ye *et al.* 2020), we reported our assessment of the skill of current global climate models for

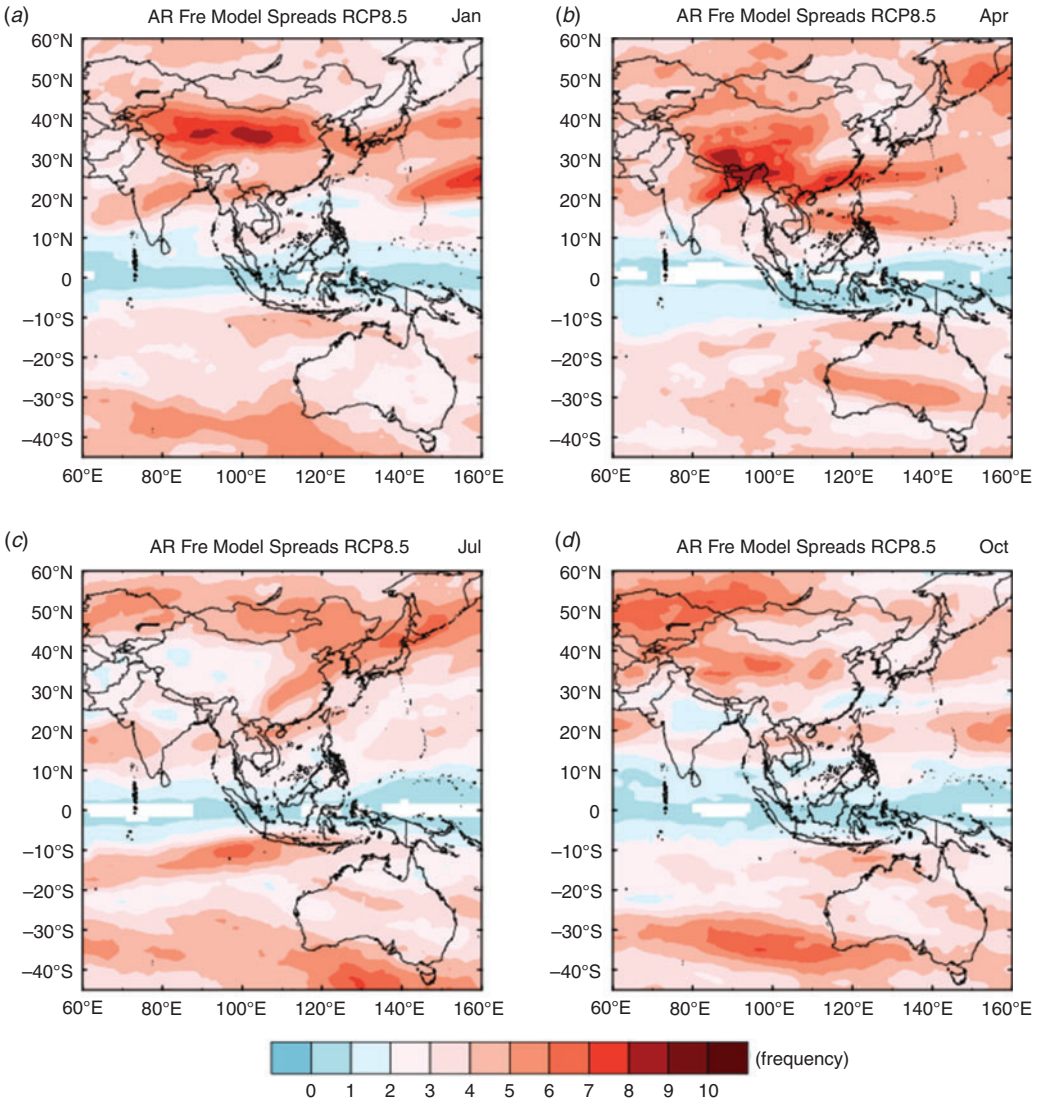


**Fig. 8.** Intermodel variations among the 17 CMIP5 for their projected changes in AR frequency, as shown in Fig. 4. It is calculated as the root-mean-square deviation from the MME, as detailed in the text.

simulating ARs under current climate conditions and their projected changes due to global warming. Despite the rapid increase in AR research in recent decades (Dettinger *et al.* 2011; Warner *et al.* 2012, 2015; Lavers *et al.* 2011, 2012; Lavers and Vilarini 2013, 2015; Garreaud 2013; Gershunov *et al.* 2017, 2019; Viale *et al.* 2018), there are relatively limited studies in the A–A monsoon region. Furthermore, published studies on future AR changes have not paid attention to the results in the A–A region (e.g. Gao *et al.* 2015; Lavers *et al.* 2015: Espinoza *et al.* 2018). But compensating effects between changes in atmospheric monsoon circulation and changes in atmospheric moisture condition responding to global warming (Zhang *et al.* 2012, 2013, 2016; Dong *et al.* 2016) could mean some different features of possible AR changes in this region.

In this study, we analysed daily IVT data from 17 CMIP5 model simulations in their historical and RCP8.5 conditions for the periods of 1981–2005 and 2081–2100. Rather than using the model reported standard pressure levels, as in some previous studies (e.g. Gao *et al.* 2015; Espinoza *et al.* 2018), in our vertical integration calculation we firstly derived the model surface pressure and then integrated from the surface up to the top of the model level. Note that, ideally, we could have used these model raw outputs at model vertical levels to do the vertical integration, but the lack of such model data in the IPCC data archive and the requirement of huge datasets to be processed for the daily IVT calculations prevented us from doing so. We then followed the objective AR detection method by Guan and Waliser (2015) to calculate the AR frequency and size in the two sets of model simulations. Considering significant seasonal variations of the monsoon climate in the A–A region, we examined the model results in January, April, July and October separately. Our key findings from this analysis were:

(i) The MME of the suite of CMIP5 models showed significant seasonal variations of horizontal water vapour

transport in the region, similar to the results derived from the reanalysis data, but their IVT magnitudes were weaker than in the reanalysis data, especially for the East Asian summer monsoon.

(ii) Because the AR detection algorithm used in our analysis was based on 85th percentile IVT, rather than a fixed threshold, the model biases in IVT magnitudes did not significantly affect our AR detections. The MME averaged AR spatial distributions and seasonal variations from these 17 models agreed well with the results derived from the reanalysis data.

(iii) Under global warming, the atmospheric water vapour transport was enhanced overall due to the increase in the atmospheric humidity. As a result, the MME also showed increased AR frequencies and bigger AR sizes in most of the A–A region, particularly over north and northeast China and the southern part of the Australian continent. These increases agreed with AR projections in North America and western Europe (e.g. Gao *et al.* 2015; Espinoza *et al.* 2018).

(iv) However, future AR changes in East Asian subtropical monsoon region can be potentially different from the changes projected for other regions. The 17 CMIP5 model ensemble results suggested some weak changes and even reduced AR frequencies and reduced AR sizes in July/August in the southern and eastern parts of China and their adjacent seas. We further investigated the underlying processes for such changes and showed that they are largely related to a westward expansion of WNPSH, as reported in other studies (Seo *et al.* 2013; Liu *et al.* 2014). This expansion resulted in a shift of south/southwesterly monsoonal flow westward toward the inland region of East Asia. At the same time, eastern China, which is normally to the west of the WNPSH and dominated by the south/southwesterly monsoon flows, was directly under the control of the westward-shifted WNPSH. This deep anticyclonic system produced dry and hot air masses and anomalous offshore winds in eastern China, and consequently, led to less frequent ARs with reduced sizes.

As the first attempt in this collaborative project to explore the potential changes of ARs in the A–A region with predicted climate warming, there are several important areas we need to strengthen in our further analyses. Firstly, our study mainly focused on the results from MME. We need to explore more details on the intermodel differences and increase our understanding of processes leading to these changes and the uncertainty in these model simulations. Although MME gave us a broad picture and consensus among the models for future projections, in future studies we can also select a few models that can skilfully simulate the A–A monsoons and ARs in the current climate and then do detailed analysis of the projected AR changes based on these model results (e.g. Dong *et al.* 2016; Zhao and Zhang 2016; Brown *et al.* 2016). Secondly, despite the fact that we were able to interpret these model results with possible underlying physical processes, we acknowledge that we only managed to examine 20-year model data, and we cannot

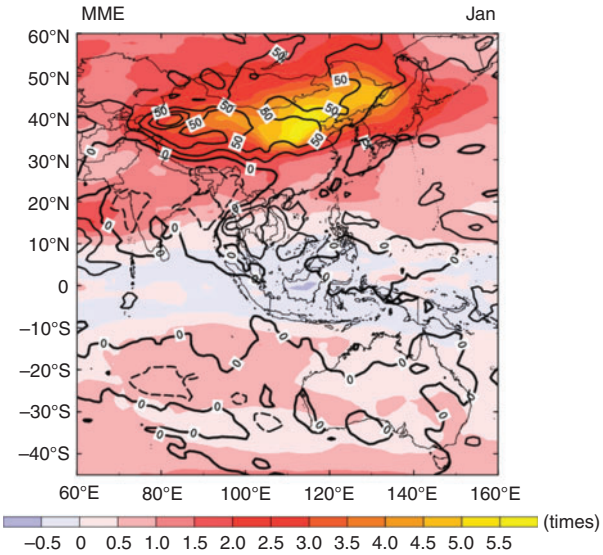


**Fig. 9.** Association of changes in the AR frequency in January, as shown in Fig. 4, which is calculated as fractional changes against the mean from historical runs (unitless; see details in Fig. 4) and the changes in Rx5day as contour lines.

attach proper statistical significance tests for the projected AR changes in the region. We also need to do more process-based analyses by decomposing the changes in ARs into changes in the atmospheric thermodynamics and dynamics, as in Gao *et al.* (2015), to further enhance our understanding of the processes resulting in changes in ARs and the associated changes in rainfall in the A–A region. Thirdly, in the context of this manuscript, we focused on the assessment of ARs and their changes in these model ensembles. In our next study, we will also focus on exploring the linkage between AR changes with changes in the rainfall intensity and distributions in the A–A region. This will be a key area of our future research. As an example, Fig. 9 shows a piece of preliminary analysis from associating changes in AR frequency in January with a rainfall extreme index, Rx5day, which represents the changes in monthly maximum consecutively over five days of precipitation. January was chosen as this month had the largest AR changes, as shown in Fig. 4, and the Rx5day index was chosen because it is one of the climate extreme indices widely used in the climate change community (ref. https://www.climdex.org/) and for studying extreme rainfall changes in East Asia (Sun and Miao 2018). In the figure, we can clearly see that in the far northeastern Asia where the AR frequency increased significantly under warmed climate, the Rx5day index also showed large increases in these regions, suggesting increased risk of more extreme winter snow storms in the region. This has significant ramifications for the social and economic development in the region. In this single manuscript, it is impossible to cover every aspect of CMIP model-simulated ARs and their changes and impacts on climate in the A–A region, but our analysis clearly shows the importance of more detailed AR studies in the region for climate change projections.

## Conflicts of interest

The authors declare that they have no conflicts of interest.

## Acknowledgements

The authors thank the Australian Bureau of Meteorology and China Meteorological Administration (CMA) for their agreement and support of this bilateral research project. H. Zhang was also supported by the Australian Government's National Environmental Science Program. We acknowledge the World Climate Research Program's Working Group on Coupled Modelling, which is responsible for CMIP, and we thank the climate modelling groups for producing and making available their model output. This study was also supported by the National Key R&D Program of China (Grant No. 2017YF0603703 and 2017YF0605004) and the second scientific research project on the Qinghai-Tibetan Plateau (2019QZKK010204) from CMA scientists involved in this study. Very constructive comments and suggestions from Drs S. Narsey and V. Kumar during the internal review process are appreciated. We also thank the two anonymous reviewers for their insightful comments and suggestion to improve the quality of this project.

## References

Brown, J., Moise, A., Colman, R., and Zhang, H. (2016). Will a warmer world mean a wetter or drier Australian monsoon? *J. Climate* **29**(12), 4577–4596. doi:10.1175/JCLI-D-15-0695.1

Chang, C. P., Harr, P. A., McBride, J., and Hsu, H.-H. (2004). Maritime Continent monsoon: Annual cycle and boreal winter variability. In 'East Asian Monsoon'. (Ed. C.-P. Chang) pp. 107–150. (World Scientific: Publishing Co. Pte. Ltd: Singapore)

Chen, J., Zhang, H., Ye, C., Chen, H., and Mo, R. (2020). Case studies of atmospheric rivers over China and Australia: new insight into their rainfall generation. *J. South. Hemisph. Earth Syst. Sci.* doi:10.1071/ES19026

Chen, L., Zhu, Q., and Luo, H. (1991). 'East Asian Monsoon'. (China Meteorological Press: Beijing, China) 362 pp [In Chinese].

Choi, W., and Kim, K.-Y. (2019). Summertime variability of the western North Pacific subtropical high and its synoptic influences on the East Asian weather. *Nature Sci. Rep.* **9**, 7865. doi:10.1038/S41598-019-44414-W

Curry, C. L., Islam, S. U., Zwiers, F. W., and Déry, S. J. (2019). Atmospheric rivers increase future flood risk in Western Canada's largest Pacific River. *Geophys. Res. Lett.* **46**, 1651–1661. doi:10.1029/2018GL080720

Dee, D. P., Uppala, S. M., Simmons, A. J., Berrisford, P., Poli, P., Kobayashi, S., Andrae, U., Balmaseda, M. A., Balsamo, G., Bauer, P., Bechtold, P., Beljaars, A. C. M., van de Berg, L., Bidlot, J., Bormann, N., Delsol, C., Dragani, R., Fuentes, M., Geer, A. J., Haimberger, L., Healy, S. B., Hersbach, H., Hólm, E. V., Isaksen, L., Kållberg, P., Köhler, M., Matricardi, M., McNally, A. P., Monge-Sanz, B. M., Morcrette, J.-J., Park, B.-K., Peubey, C., de Rosnay, P., Tavolato, C., Thépaut, J.-N., and Vitart, F. (2011). The ERA-Interim reanalysis: configuration and performance of the data assimilation system. *Quart. J. Roy. Meteorol. Soc.* **137**, 553–597. doi:10.1002/QJ.828

Dettinger, M. D., Ralph, F. M., Das, T., *et al.* (2011). Atmospheric rivers, floods, and the water resources of California. *Water* **3**, 445–478. doi:10.3390/W3020445

Ding, Y. (2004). Seasonal march of the East-Asian summer monsoon. In 'East Asian Monsoon'. (Ed. C.-P. Chang) pp. 3–53. (World Scientific Publishing Co. Pte. Ltd: Singapore)

Ding, Y., Liang, P., Liu, Y., and Zhang, Y. (2020). Multiscale variability of Meiyu and its prediction: A new review. *J. Geophys. Res.* **125**, e2019JD031496. doi:10.1029/2019JD031496

Dong, G., Zhang, H., Moise, A., Hanson, L., Liang, P., and Ye, H. (2016). CMIP5 model-simulated onset, duration and intensity of the Asian summer monsoon in current and future climate. *Clim. Dyn.* **46**, 355–382. doi:10.1007/S00382-015-2588-Z

Espinoza, V., Waliser, D. E., Guan, B., Lavers, D. A., and Ralph, F. M. (2018). Global analysis of climate change projection effects on atmospheric rivers. *Geophys. Res. Lett.* **45**, 4299–4308. doi:10.1029/2017GL076968

Gao, Y., Lu, J., Leung, L. R., Yang, Q., Hagos, S., and Qian, Y. (2015). Dynamical and thermodynamical modulations on future changes of landfalling atmospheric rivers over western North America. *Geophys. Res. Lett.* **42**, 7179–7186. doi:10.1002/2015GL065435

Garreaud, R. (2013). Warm winter storms in central Chile. *J. Hydrometeor* **14**, 1515–1534. doi:10.1175/JHM-D-12-0135.1

Gershunov, A., Shulgina, T., Ralph, F. M., Lavers, D. A., and Rutz, J. J. (2017). Assessing the climate-scale variability of atmospheric rivers affecting western North America. *Geophys. Res. Lett.* **44**, 7900–7908. doi:10.1002/2017GL074175

Gershunov, A., Shulgina, T., Clemesha, R. E. S., Guirguis, K., Pierce, D. W., Dettinger, M. D., Lavers, D. A., Cayan, D. R., Polade, S. D., Kalansky, J., and Ralph, F. M. (2019). Precipitation regime change in western North America: The role of atmospheric rivers. *Sci. Rep.* **9**, 9944. doi:10.1038/S41598-019-46169-W

Guan, B., and Waliser, D. E. (2015). Detection of atmospheric rivers: evaluation and application of an algorithm for global studies. *J. Geophys. Res.* **120**, 12514–12535. doi:10.1002/2015JD024257

He, C., and Zhou, T. (2015). Responses of the Western North Pacific subtropical high to global warming under RCP4.5 and RCP8.5 scenarios projected by 33 CMIP5 models: The dominance of tropical Indian Ocean–tropical Western Pacific SST gradient. *J. Climate* **28**, 365–380. doi:10.1175/JCLI-D-13-00494.1

He, C., Zhou, T., Lin, A., Wu, B., Gu, D., Li, C., and Zheng, B. (2015). Enhanced or weakened western North Pacific subtropical high under global warming? *Nature Sci. Rep.* **5**, 16771. doi:10.1038/SREP16771

Hirota, N., Takayabu, Y. N., Kato, M., and Arakane, S. (2016). Roles of an atmospheric river and a cutoff low in the extreme precipitation event in Hiroshima on 19 August 2014. *Mon. Wea. Rev.* **144**, 1145–1160. doi:10.1175/MWR-D-15-0299.1

IPCC (2007). Climate Change 2007: The Physical Science Basis. Working Group I Contribution to the Fourth Assessment Report of the Intergovernmental Panel on Climate Change. (Eds S. D. Solomon, D. Qin, M. Manning, Z. Chen, M. Marquis, K. B., Avery, M. Tignor and H. L. Miller). Cambridge University Press, Cambridge, United Kingdom and New York, NY, USA, 996 pp.

IPCC (2013). Climate Change 2013: The Physical Science Basis. Contribution of Working Group I to the Fifth Assessment Report of the Intergovernmental Panel on Climate Change. (Eds T. F. Stocker, D. Quin, G.-K., Plattner, M. Tignor, S. K. Alen, J. Boschung, A. Nauels, Y. Xia, V. Bex and P. M. Midgley). Cambridge University Press, Cambridge, United Kingdom and New York, NY, USA, 1535 pp.

Jeon, S., Prabhat, Byna, S., Gu, J., Collins, W. D., and Wehner, M. F. (2015). Characterization of extreme precipitation within atmospheric river events over California. *Adv. Stat. Clim. Meteorol. Oceanogr.* **1**, 45–57. doi:10.5194/ASCMO-1-45-2015

Jiang, D., and Tian, Z. (2013). East Asian monsoon change for the 21st century: Results of CMIP3 and CMIP5 models. *Chinese Sci. Bull.* **58**, 1427–1435. doi:10.1007/S11434-012-5533-0

Jiang, D., Tian, Z., and Lang, X. (2016). Reliability of climate models for China through the IPCC Third to Fifth Assessment Reports. *Int. J. Climatol.* **36**, 1114–1133. doi:10.1002/JOC.4406

Kamae, Y., Mei, W., and Xie, S.-P. (2019). Ocean warming pattern effects on future changes in East Asian atmospheric rivers. *Environ. Res. Lett.* **14**, 054019. doi:10.1088/1748-9326/AB128A

Kitoh, A. (2017). The Asian monsoon and its future change in climate models: A review. *J. Meteorol. Soc. Japan*. doi:10.2151/JMSJ.2017-002

Lavers, D. A., Allan, R. P., Wood, E. F., Villarini, G., Brayshaw, D. J., and Wade, A. J. (2011). Winter floods in Britain are connected to atmospheric rivers. *Geophys. Res. Lett.* **38**, L23803. doi:10.1029/2011GL049783

Lavers, D. A., Villarini, G., Allan, R. P., Wood, E. F., and Wade, A. J. (2012). The detection of atmospheric rivers in atmospheric reanalyses and their links to British winter floods and the large-scale climatic circulation. *J. Geophys. Res. Atmos.* **117**, D20106. doi:10.1029/2012JD018027

Lavers, D. A., and Villarini, G. (2013). The nexus between atmospheric rivers and extreme precipitation across Europe. *Geophys. Res. Lett.* **40**(12), 3259–3264. doi:10.1002/GRL.50636

Lavers, D. A., Allan, R. P., Villarini, G., Lloyd-Hughes, B., Brayshaw, D. J., and Wade, A. J. (2013). Future changes in atmospheric rivers and their implications for winter flooding in Britain. *Environ. Res. Lett.* **8**, 034010. doi:10.1088/1748-9326/8/3/034010

Lavers, D. A., and Villarini, G. (2015). The contribution of atmospheric rivers to precipitation in Europe and the United States. *J. Hydrol.* **522**, 382–390. doi:10.1016/J.JHYDROL.2014.12.010

Lavers, D. A., Ralph, F. M., Waliser, D. E., Gershunov, A., and Dettinger, M. D. (2015). Climate change intensification of horizontal water vapor transport in CMIP5. *Geophys. Res. Lett.* **42**, 5617–5625. doi:10.1002/2015GL064672

Li, B., and Zhou, T. (2010). Projected Climate Change over China under SRES A1B Scenario: Multi-model Ensemble and Uncertainties. *Adv. Climate Change Res.* **6**(4), 270J276. [In Chinese].

Li, X., Ting, M., Li, C., and Henderson, N. (2015). Mechanisms of Asian summer monsoon changes in response to anthropogenic forcing in CMIP5 models. *J. Climate* **28**, 4107–4125. doi:10.1175/JCLI-D-14-00559.1

Liang, P., Dong, G., Zhang, H., Zhao, M., and Ma, Y. (2020). Atmospheric rivers associated with summer heavy rainfall over the Yangtze Plain. *J. South. Hemisph. Earth Syst. Sci.* doi:10.1071/ES19028

Liu, Y., Li, W., Zuo, J., and Hu, Z.-Z. (2014). Simulation and projection of the western Pacific subtropical high in CMIP5 models. *J. Meteorol. Res.* **28**, 327–340. doi:10.1007/S13351-014-3151-2

Mahoney, K., Jackson, D. L., Neiman, P. J., Hughes, M., Darby, L., Wick, G., White, A. B., Sukovich, E., and Cifelli, R. (2016). Understanding the role of atmospheric rivers in heavy precipitation in the southeast United States. *Mon. Wea. Rev.* **144**, 1617–1632. doi:10.1175/MWR-D-15-0279.1

Mo, R., Brugman, M. M., Milbrandt, J. A., Goosen, J., Geng, Q., Emond, C., Bau, J., and Erfani, A. (2019). Impacts of hydrometeor drift on orographic precipitation: Two case studies of landfalling atmospheric rivers in British Columbia, Canada. *Wea. Forecasting* **34**, 1211–1237. doi:10.1175/WAF-D-18-0176.1

Mo, R., and Lin, H. (2019). Tropical–mid-latitude interactions: Case study of an inland-penetrating atmospheric river during a major winter storm over North America. *Atmos.-Ocean* **57**, 208–232. doi:10.1080/07055900.2019.1617673

Narsey, S., Reeder, M. J., Ackerley, D., and Jakob, C. (2017). A Midlatitude Influence on Australian Monsoon Bursts. *J. Climate* **30**, 5377–5393. doi:10.1175/JCLI-D-16-0686.1

Neiman, P. J., Ralph, F. M., Wick, G. A., Lundquist, J., and Dettinger, M. D. (2008*a*). Meteorological characteristics and overland precipitation impacts of atmospheric rivers affecting the West Coast of North America based on eight years of SSM/I satellite observations. *J. Hydrometeor.* **9**, 22–47. doi:10.1175/2007JHM855.1

Neiman, P. J., Ralph, F. M., Wick, G. A., Kuo, Y.-H., Wee, T.-K., Ma, Z., Taylor, G. H., and Dettinger, M. D. (2008*b*). Diagnosis of an intense atmospheric river impacting the Pacific Northwest: Storm summary and offshore vertical structure observed with COSMIC satellite retrievals. *Mon. Wea. Rev.* **136**, 4398–4420. doi:10.1175/2008MWR2550.1

Paltan, H., Waliser, D., Lim, W. H., Guan, B., Yamazaki, D., Pant, R., and Dadson, S. (2017). Global floods and water availability driven by atmospheric rivers. *Geophys. Res. Lett.* **44**, doi:10.1002/2017GL074882

Payne, A. E., Demory, M.-E., Leung, L. R., Ramos, A. M., Shields, C. A., Rutz, J. J., Siler, N., Villarini, G., Hall, A., and Ralph, F. M. (2020). Responses and impacts of atmospheric rivers to climate change. *Nat. Rev. Earth Environ.* **1**, 143–157. doi:10.1038/S43017-020-0030-5

Radić, V., Cannon, A. J., Menounos, B., and Gi, N. (2015). Future changes in autumn atmospheric river events in British Columbia, Canada, as projected by CMIP5 global climate models. *J. Geophys. Res. Atmos.* **120**, 9279–9302. doi:10.1002/2015JD023279

Ralph, F. M., Neiman, P. J., and Wick, G. A. (2004). Satellite and CALJET aircraft observations of atmospheric rivers over the eastern North Pacific Ocean during the winter of 1997/98. *Mon. Wea. Rev.* **132**, 1721–1745. doi:10.1175/1520-0493(2004)132<1721:SACAOO>2.0.CO;2

Ralph, F. M., Neiman, P. J., Wick, G. A., Gutman, S. I., Dettinger, M. D., Cayan, D. R., and White, A. B. (2006). Flooding on California's Russian River: role of atmospheric rivers. *Geophys Res Lett* **33**, L13801. doi:10.1029/2006GL026689

Ralph, F. M., Dettinger, M., Lavers, D., Gorodetskaya, I. V., Martin, A., Viale, M., White, A. B., Oakley, N., Rutz, J., and Spackman, J. R. (2017). Atmospheric rivers emerge as a global science and applications focus. *Bull. Amer. Meteor. Soc.* **98**, 1969–1973. doi:10.1175/BAMS-D-16-0262.1

Ramos, A. M., Tomé, R., Trigo, R. M., Liberato, M. L. R., and Pinto, J. G. (2016). Projected changes in atmospheric rivers affecting Europe in CMIP5 models. *Geophys. Res. Lett.* **43**, 9315–9323. doi:10.1002/2016GL070634

Seo, K.-H., Ok, J., Son, J.-H., and Cha, D.-H. (2013). Assessing Future Changes in the East Asian Summer Monsoon Using CMIP5 Coupled Models. *J. Climate* **26**, 7662–7675. doi:10.1175/JCLI-D-12-00694.1

Shields, C. A., Rutz, J. J., Leung, L.-Y., Ralph, F. M., Wehner, M., Kawzenuk, B., Lora, J. M., McClenny, E., Osborne, T., Payne, A. E., Ullrich, P., Gershunov, A., Goldenson, N., Guan, B., Qian, Y., Ramos, A. M., Sarangi, C., Sellars, S., Gorodetskaya, I., Kashinath, K., Kurlin, V., Mahoney, K., Muszynski, G., Pierce, R., Subramanian, A. C., Tome, R., Waliser, D., Walton, D., Wick, G., Wilson, A., Lavers, D., Prabhat, Collow, A., Krishnan, H., Magnusdottir, G., and Nguyen, P. (2018). Atmospheric River tracking method intercomparison project (ARTMIP): Project goals and experimental design. *Geosci. Model Dev.* **11**, 2455–2474. doi:10.5194/GMD-11-2455-2018

So, S. S., Lee, C. W., Kim, M. K., and So, E. M. (1994). Atmospheric Observation, Kyomun Press in Korean.

Sun, Q., and Miao, C. (2018). Extreme rainfall (R20mm, RX5day) in Yangtze–Huai, China, in June–July 2016: The role of ENSO and anthropogenic climate change. *Bull. Amer. Meteor. Soc.* **99**, S102–S106. doi:10.1175/BAMS-D-17-0091.1

Taylor, K. E., Stouffer, R. J., and Meehl, G. A. (2012). An overview of CMIP5 and the experiment design. *Bull. Amer. Meteor. Soc.* **93**, 485–498. doi:10.1175/BAMS-D-11-00094.1

Viale, M., Valenzuela, R., Garreaud, R. D., and Ralph, F. M. (2018). Impacts of atmospheric rivers on precipitation in southern South America. *J. Hydrometeor.* **19**, 1671–1687. doi:10.1175/JHM-D-18-0006.1

Wang, B. (2006). 'The Asian monsoon'. (Praxis Publishing: Chichester, UK). 787 pp.

Warner, M. D., Mass, C. F., and Salathé, E. P., Jr (2012). Wintertime extreme precipitation events along the Pacific Northwest coast: Climatology and synoptic evolution. *Mon. Wea. Rev.* **140**, 2021–2043. doi:10.1175/MWR-D-11-00197.1

Warner, M. D., Mass, C. F., and Salathé, E. P. (2015). Changes in winter atmospheric rivers along the North American West Coast in CMIP5 climate models. *J. Hydrometeor.* **16**, 118–128. doi:10.1175/JHM-D-14-0080.1

Wick, G. A. (2014). Implementation and initial application of an atmospheric river detection tool based on integrated vapor transport. American Geophysical Union 2014 Fall Meeting, San Francisco, Abstract A34E-06.

Wu, X., Ye, C., He, W., Chen, J., Xu, L., and Zhang, H. (2020). Atmospheric rivers impacting mainland China and Australia: climatology and interannual variations. *J. South. Hemisph. Earth Syst. Sci.* doi:10.1071/ES19029

Xu, L., Zhang, H., He, W., Ye, C., and Moise, A. (2020). Potential connections between atmospheric rivers in China and Australia. *J. South. Hemisph. Earth Syst. Sci.* doi:10.1071/ES19027

Yang, Y., Zhao, T., Ni, G., and Sun, T. (2018). Atmospheric rivers over the Bay of Bengal lead to northern Indian extreme rainfall. *Int. J. Climatol.* **38**, 1010–1021. doi:10.1002/JOC.5229

Ye, C., Zhang, H., Moise, A., and Mo, R. (2020). Atmospheric rivers in the Australia-Asian region: a BoM–CMA collaborative study. *J. South. Hemisph. Earth Syst. Sci.* doi:10.1071/ES19025

Zhang, C. J., and Zhang, H. (2010). Potential impacts of east Asian winter monsoon on climate variability and predictability in the Australian summer monsoon region. *Theor. Appl. Climatol.* **101**, 161–177. doi:10.1007/S00704-009-0246-2

Zhang, H. (2010). Diagnosing Australia-Asian monsoon onset/retreat using large-scale wind and moisture indices. *Clim. Dyn.* **35**, 601–618. doi:10.1007/S00382-009-0620-X

Zhang, H., Qin, J., and Li, Y. (2011). Climatic background of cold and wet winter in southern China: part I observational analysis. *Clim. Dyn.* **37**, 2335–2354. doi:10.1007/S00382-011-1022-4

Zhang, H., Liang, P., Moise, A., and Hanson, L. (2012). Diagnosing potential changes in Asian summer monsoon onset and duration in IPCC AR4 model simulations using moisture and wind indices. *Clim. Dyn.* **39**, 2465–2486. doi:10.1007/S00382-012-1289-0

Zhang, H., Moise, A., Liang, P., and Hanson, L. (2013). The response of summer monsoon onset/retreat in Sumatra-Java and tropical Australia region to global warming in CMIP3 models. *Clim. Dyn.* **40**, 377–399. doi:10.1007/S00382-012-1389-X

Zhang, H., Dong, G., Moise, A., Colman, R., Hanson, L., and Ye, H. (2016). Uncertainty in CMIP5 model-projected changes in the onset/retreat of the Australian summer monsoon. *Clim. Dyn.* **46**, 2371–2389. doi:10.1007/S00382-015-2707-X

Zhang H., and Moise, A. (2016). The Australian summer monsoon in current and future climate. In 'The Monsoons and Climate Change' (Eds L. M. V. de Carvalho, C. Jones) pp. 67–120. (Springer International Publishing: Cham, Switzerland)

Zhao, Y., and Zhang, H. (2016). Impacts of SST warming in tropical Indian Ocean on CMIP5 model-projected summer rainfall changes over Central Asia. *Clim. Dyn.* **46**, 3223–3238. doi:10.1007/S00382-015-2765-0

Zhou, T., Yu, R., Zhang, J., *et al.* (2009). Why the Western Pacific subtropical high has extended westward since the late 1970s. *J. Climate* **22**, 2199–2215. doi:10.1175/2008JCLI2527.1

Zhu, Y., and Newell, R. E. (1994). Atmospheric rivers and bombs. *Geophys. Res. Lett.* **21**, 1999–2002. doi:10.1029/94GL01710

Zhu, Y., and Newell, R. E. (1998). A proposed algorithm for moisture fluxes from atmospheric rivers. *Mon. Wea. Rev.* **126**, 725–735. doi:10.1175/1520-0493(1998)126<0725:APAFMF>2.0.CO;2